P3M.2 AN INVESTIGATION OF TURBULENT PROCESSES IN THE LOWER STRATOSPHERE

Chad J. Ringley*, Yuh-Lang Lin, P.S. Suffern
North Carolina State University, Raleigh, NC

Michael L. Kaplan
Desert Research Institute, Reno, NV

1. INTRODUCTION

The turbulent kinetic energy (TKE) tendency equation is widely applied to quantify turbulent tendency and eddy dissipation rate (EDR) within the planetary boundary layer (PBL). Due to the complexity that arises from Reynolds averaging, various approximation parameters, as described by Yamada and Mellor (1975) and Stull (1988), are often used to approximate the TKE tendency equation for idealized, measured, or simulated data. The application of the TKE tendency equation as a closed, solvable system is most common within the PBL, where friction and surface heating drive turbulent motion.

Though the strongest turbulent motions are, on average, confined to the PBL, turbulence is experienced at vertical levels well above the lowest 2 kilometers. Many previous authors have examined the effects of both convectively and orgraphically-induced gravity waves on turbulence well into the stratosphere. Lane et al. (2003) found a regime of turbulence just above the initial overshooting top associated with deep convection. In addition, Lane et al. (2003) described the gravity wave breakdown that occurred as high as 3 kilometers above the tropopause as another regime of turbulent motion. Both convectively and orgraphically-induced gravity waves are able to propagate well into the stratosphere due to the presence of high static stability and can reach heights that may threaten high-altitude flying aircraft. Lilly and Lester (1974) used observational data from aircraft to reveal sporadically-turbulent gravity waves generated by terrain over southern Colorado that reached heights of up to 17 kilometers. Leutbecher and Volkert (2000) performed a numerical simulation of an aircraft-related turbulence incident linked to orgraphically-induced gravity waves with heights up to 20 kilometers.

*The breaking of a vertically propagating gravity wave would introduce the greatest threat to high-altitude flying aircraft, such as spy planes. Because there exists no prescribed limitation on where the TKE tendency equation is used, high vertical and horizontal resolution model simulations with high output frequency can be used to quantify individual terms within the TKE tendency equation with 1.5-degree closure at any level within the atmosphere. The purpose of this study is to apply the TKE tendency equation using a series of Reynolds averaging techniques in order to approximate TKE tendency associated with a vertically propagating gravity wave in the lower and middle stratosphere. By calculating each term in the TKE tendency equation explicitly, the study will help provide insight on the important physical processes related to turbulence generation due to wave breaking.

* *Corresponding author address:* Chad J. Ringley, NC State University, Dept. of Marine, Earth, & Atmos. Sciences, Raleigh, NC 27606. e-mail: chad_ringley@ncsu.edu

2. METHODOLOGY

From Stull (1988), the TKE tendency equation can be written as:

$$\frac{\partial \bar{e}}{\partial t} = -\bar{u}\frac{\partial \bar{e}}{\partial x} - \bar{v}\frac{\partial \bar{e}}{\partial y} - \bar{w}\frac{\partial \bar{e}}{\partial z} + \frac{g}{\bar{\theta}_v}\overline{(w'\theta_v')} - \overline{(u'w')}\frac{\partial \bar{u}}{\partial z} - \frac{\partial}{\partial z}(\overline{w'e}) - \frac{1}{\bar{\rho}}\frac{\partial}{\partial z}(\overline{w'p'}) - \varepsilon \quad (1)$$

The form of the TKE tendency equation given in (1) does not require horizontal homogeneity as prescribed by Stull (1988). The terms on the right hand side of (1) are hereafter characterized by the definitions proposed by Stull (1988) and are as follows: the first three terms are the horizontal and vertical advection of TKE by the mean wind, the fourth term is buoyant production, the fifth term is mechanical shear, the sixth term is turbulent transport, the seventh term is pressure perturbations, and the eighth term is TKE dissipation or EDR. The form is very similar to the TKE tendency equation used in Kiefer (2005) with the addition of the horizontal advection terms.

The dependent variables on the right hand side of (1) are all known from the output of a numerical model simulation. A simple Reynolds averaging technique is used, represented by:

$$\Omega' = \Omega - \bar{\Omega} \quad (2)$$

where Ω represents any of the dependent variables (u,v,w, etc.) directly output from the model at each time step. The period over which the Reynolds averaging is performed will be varied in order to find the best structural representation of the vertically propagating gravity wave. Vertical and horizontal derivatives are calculated using a 2nd-order centered finite difference scheme obtained from the

model grids within the simulations. A series of programs and scripts were added to the normal model post-processing routine in order to perform the Reynolds averaging calculations and calculate each term independently.

3. MODEL SIMULATIONS

On 12 December 2002, a large amplitude surface gravity wave initiated deep moist convection over Eastern Texas and Western Louisiana. Figure 1 shows the surface gravity wave signature from a microbarogram in Palestine, TX. The "wave of depression" corresponds to 6-millibar pressure fall in a two-hour period near 2230 UTC 12 December 2002. A complete synoptic and mesoscale discussion of the parameters leading to the development of the event can be found in Suffern et al. (2005).

The convection generated due to the surface gravity wave became the subject of several high-resolution model simulations using the Non-Hydrostatic Stratospheric Mesoscale Atmospheric Simulation System, hereafter *Strato-NHMASS*. Figure 2 shows the model domain configurations for the Strato-NHMASS simulations over Eastern Texas and Western Louisiana. In order to better resolve the scales of motion required to accurately diagnose TKE tendency, several extremely high-resolution simulations were performed over a small portion of eastern Jasper and western Newton counties in southeastern Texas. The Strato-NHMASS simulations used a one-way nesting algorithm, starting with an 18-kilometer (km) simulation initialized with NCEP reanalysis data (1°x1°) resolution. Model simulations with horizontal resolutions of 6 km, 2 km, 667 meters, 222 meters, and 71 meters were performed using the one-way nesting algorithm (Fig. 2). All simulations were run using a 162x162 grid, the Kain-Fritch convective parameterization scheme and Lin et al. (1983) microphysics package. The model was run with a TKE PBL option, and the TKE from the model is used in the calculations represented in (1).

The horizontal and vertical grid structures must be of comparable resolution in order to capture the wave in full detail. For this reason, the TKE and EDR calculations are only applied to the 222-meter and 71-meter simulations in the study. The Strato-NHMASS model is run with 90-σ levels extending up to 10 millibars. Data from σ–levels above the 300-millibar level were interpolated into height coordinates with a 250-meter vertical resolution, closely matching the horizontal grid dimensions. The TKE calculations are then performed from the 300-millibar (around 9 kilometer) to 10-millibar (around 21 kilometer) levels.

In addition to the different horizontal resolutions used for the 12 December 2002 case, different Reynolds averaging periods were used. First, the entire duration of the model simulation was averaged, and perturbations were derived from this 1-segment averaged model run simulations. The model output was also averaged in four equally spaced temporal segments (hereafter, 4-segment), which allows for higher frequency modes to be captured when compared to the 1-segment TKE budget.

4. RESULTS

4.1 *12 December 2002 Strato-NHMASS 222-meter Simulation, 1-Segment Budget*

The 222-meter simulation was initialized at 2209 UTC 12 December 2002 using the data from the 667-meter simulation. The convection generated by the surface-based gravity wave (shown in Figure 3) was already present in the initial conditions within the first guess field of the 222-meter run. The model time step was 0.07 seconds, and data was output every 54 seconds during the 35 minute, 6 second simulation. As described in Section 3, the entire 35 minute, 6 second model run was averaged, and perturbations calculated using (2). Figure 4 shows a four-panel plot of the u-prime field using the 1-segment averaging technique. In the perturbation fields, the vertically propagating gravity wave is seen amplifying until reaching the 16-18 km level (Fig. 4c) and breaking shortly thereafter (Fig. 4d), between 20 and 25 minutes into the simulation (valid 2230-2236 UTC 12 December 2002). Though not shown in this manuscript, perturbation values from the v and w wind fields also showed a similar wave structure. In addition to the kinematic perturbation field, investigation of the thermodynamic perturbation field (virtual potential temperature) also showed a distinct wave signature. Figure 5 shows a four-panel plot of the θ-v field using the 1-segment averaging technique. Perturbations with a range from –20 to 20 Kelvin (Fig. 5c) suggest that the buoyant production/destruction of TKE play a significance role with the vertically propagating stratospheric wave.

Linear gravity wave theory suggests that the critical level, the level in which the stratospheric wave would break, would be found where the forward speed of the propagating gravity wave is equal to the local flow speed. Graphical analysis suggests that a forward speed of U = 16 meters per second would roughly correspond to a critical level lying between 16-18 km between 2230-2236 UTC. A power spectrum analysis will be required to find the exact location of the critical level at the time of the wave break, but it is theorized that the critical level will fall within the 16.5-18 km range, consistent

with the findings of Lane et al. (2003).

Once the perturbations and time averages were calculated, each individual term in (1) was calculated for the 1-segment averaged data. The first three terms on the right hand side of (1), representing the horizontal and vertical advection of TKE by the mean wind (not shown), was small in comparison to the buoyant production and mechanical shear terms in (1). The most likely explanation for the negligible TKE profile contributions from the advection terms is from the Reynolds averaging technique. High frequency shifts in momentum may have been averaged out, and short-lived TKE gradients may also have been averaged out. This issue will be revisited with the 4-segment TKE budget presented in Section 4.2.

The two most important term contributions to the overall TKE tendency were the buoyant production and mechanical shear. Figure 6a is the 1-segment TKE budget average for the buoyancy production term, the fourth term in (1). A distinct couplet in the buoyancy term is located between the 16-17 km level, very close to the same geographical location in the cross-section showing the breaking stratospheric wave (Fig. 4c). Figure 6b is the 1-segment TKE budget average for mechanical shear, the fifth term in (1). As with Fig. 6a, a distinct couplet in contribution from mechanical shear is found in the 16-17 km level. Contributions from the other terms in (1) (not shown) were not of the same order of magnitude as the buoyancy and mechanical shear term.

4.2 *12 December 2002 Strato-NHMASS 222-meter Simulation, 4-Segment Budget*

To further enhance the Reynolds averaging skill in more accurately resolving temporal features within the event, the averaging time was split into four separate, equally sorted time periods. With model output available every 54 seconds, four separate averaging time periods were used, each lasting 9 minutes each. The time structure of the averaging means that 10 model output times were averaged for each dependent variable, allowing for a fairly representative depiction of the wave during each segment. The patterns depicted in the 4-segment budget perturbation fields show the same wave structure (as in Fig. 4 and Fig, 5) but exhibit a slightly higher-frequency signal than the 1-segment budget. As with the 1-segment budget in Section 4.1, the buoyancy production and mechanical shear terms were dominant in the TKE contribution.

However, the higher frequency temporal averaging did improve the contribution signal from a number of other terms. Figures 7 and 8 show four-panel plots of TKE profile contribution from w-advection (Fig. 7) and buoyancy production (Fig. 8). Other term contributions are not shown due to space limits. Each term shows a similar vertical structure mimicking the vertical wave structure shown in Fig. 4. The highest values of TKE contribution come in the final two averaging periods between 2227-2245 UTC 12 September 2002, after the stratospheric wave has broken. Most of the terms also show a distinct couplet in TKE creation/destruction between the 16-18 km layer, consistent with the 1-segment averaging shown in Section 4.1. The higher frequency temporal signature given by the 4-segment averaging technique shows promise in depicting the structure of vertically propagating gravity waves through both perturbation and term fields, and locating areas of TKE creation/destruction well into the stratosphere.

4.3 *12 December 2002 Strato-NHMASS 71-meter Simulation*

The 222-meter simulation discussed in Sections 4.1 and 4.2 was then used to initialize the Strato-NHMASS model to run at a 71-meter vertical resolution, as shown in the domain map in Fig. 1. Using the same methodology outlined previously, the 71-meter simulation was subjected to both Reynolds averaging techniques (1-segment and 4-segment). The 1-segment TKE budget uses an entire model simulation time of 13.5 minutes. The 4-segment TKE budget uses four equally spaced averaging periods that are 2.5 minutes long with model output that was available every 30 seconds.

Unlike the 222-meter simulation, the TKE profile contribution from the first three advective terms was as large as the buoyant production and mechanical shear terms. Figure 9 shows a three-panel plot of TKE contribution from u-mean, v-mean, and w-mean advection terms in (1) for the 71-meter simulation. As with the 222-m 1-segment TKE budget, the same vertical level (16-18 km) and geographical location in the cross-section are identified, but with much higher values. Further analysis of the horizontal and vertical TKE gradients (not shown) identified stronger TKE gradients as the main factor, consistent with the higher model resolution. Figure 10 shows a three-panel plot of TKE contribution from buoyant production, mechanical shear, and turbulent transport. Though contributions from the mechanical shear and turbulent transport terms are not as pronounced as the advection or buoyant production terms, the plots show a higher-frequency signature consistent with smaller waves and perturbations in the 71-meter simulation, and again correspond to the same three-dimensional location discussed in Sections 4.1 and 4.2.

The 4-segment TKE budget graphics for the 71-meter simulation are to be completed for the presentation, but are not shown here. The 4-

segment 71-meter simulation had similar quantitative values and vertical structure comparable with the 1-segment results, but with a higher temporal frequency signature, and is consistent with the findings for the 222-meter simulations discussed in Section 4.2.

5. CONCLUSIONS AND FUTURE WORK

A Reynolds averaging approach to the TKE tendency equation is applied to a convectively induced vertically propagating gravity wave in the lower and middle stratosphere. Each term in the TKE tendency equation is calculated explicitly for two high-resolution model runs (222-meter and 71-meter) using different averaging techniques and a vertical resolution of 250-meters. The Strato-NHMASS model, with 90 vertical levels and a model lid at 10 millibars, is used to simulate the stratospheric waves. The case used to investigate the formulation is the 12 December 2002 large amplitude gravity wave case described in detail by Suffern et al. (2005).

The two different averaging techniques (1-segment and 4-segment) are done for a 35 minute, 6 second run at a horizontal resolution of 222-meters for the 12 December 2002 case. The perturbation field associated revealed the level of wave-breaking to be between the 16-18 kilometer level 20 minutes into the simulation. Graphical interpretation of the data also suggests that this level and time period is likely also the region of the critical level. The stratospheric wave broke in under the same conditions and in the same manner consistent with the idealized simulations of Lane et al. (2003), though a power spectrum analysis is needed to verify this quantitatively.

The 1-segment 222-meter TKE budget identified the geographical location in three-dimensional space of the breaking wave in the stratosphere through the TKE term contributions; specifically the buoyancy production and mechanical shear terms. The results suggest that buoyancy production and mechanical shear production of turbulence are the most important contributor to TKE profiles on a 35-minute time scale, and are highest in the region of stratospheric wave breaking (or the critical level). The 4-segment 222-meter TKE budget had a much higher temporal frequency than with the 1-segment budget, consistent with the shorter averaging times. As was with the 1-segment budget, the buoyancy production and mechanical shear terms provided the greatest contribution.

The 222-meter simulation was used to initialize another Strato-NHMASS run for the 12 December 2002 case. A horizontal resolution of 71-meters was used to simulate a very small area over Easter Jasper and Western Newton County in southeast Texas. The model run was subjected to both the 1-segment and 4-segment TKE budget approach. The 1-segment TKE budget revealed non-negligible TKE contributions from the advection terms and a much stronger TKE signal in general. Investigation of the TKE gradients within the 71-meter simulation showed much stronger gradients, implying that the model grid resolution is an important factor in determining term contributions. For a very small temporal and spatial scale, the authors hypothesize that contributions from the advection terms in the TKE tendency equation are non-negligible, and must be taken into consideration depending on the scale of the event. Though not shown in the manuscript, EDR profiles have been computed for a few simulations, and will be incorporated into an automated nesting algorithm that will use the EDR values calculated from the TKE tendency equation rather than from the parameterizations built in to the model.

The convectively induced vertically propagating gravity wave from the 12 December 2002 shows turbulence characteristics similar to classical orgraphically-induced gravity waves that have been studied in great detail. Because the time scales in the model simulations are short, the convective updraft is, for all practical purposes, quasi-stationary. The possibility exists that one can treat the updraft as a quasi-stationary, diabatic “mountain”, with the same wave generation and turbulence profiles as that of a true orographic feature. Future study includes an identical analysis for a vertically propagating gravity wave induced by a true mountain and comparison to other modes of convection.

6. ACKNOWLEDGMENTS

This research was supported under U.S. Air Force contract FA8718-04-C-0011. The main author wishes to thank Dr. Michael Brennan, Michael Kiefer, Zachary Brown and Chris Hill for their helpful input, and Nicole Haglund and Emily Lunde for helpful manuscript suggestions.

7. REFERENCES

Kiefer, M.T., 2005: The Impact of Superimposed Synoptic to Meso-Gamma Scale Motions on Extreme Snowfall over western Maryland and northeast West Virginia during the 2003 President’s Day winter storm. MS thesis, Dept. of Marine, Earth, and Atmospheric Sciences, North Carolina State University, 204 pp.

Lane, Todd P., Sharman, Robert D., Clark, Terry L., Hsu, Hsiao-Ming, 2003: An Investigation of Turbulence Generation Mechanisms

above Deep Convection. *J. Atmos. Sci.,* **60,** 1297-1321.

Leutbecher, Martin and Hans Volkert. 2000: The Propagation of Mountain Waves into the Stratosphere: Quantitative Evaluation of Three-Dimensional Simulations. *J. Atmos. Sci.*: **57**, 3090–3108.

Lilly, D.K. and Peter F. Lester. 1974: Waves and Turbulence in the Stratosphere. *J. Atmos. Sci.*: **31**, 800–812.

Stull, Roland B., 1988: *An Introduction to Boundary Layer Meteorology***.** Kluwer Academic Press: 639 pp.

Suffern, P.S., 2005: Numerical Simulations of Vertically Propagating Gravity Waves in the Stratosphere Above a Hydrostatic Large Amplitude Surface Gravity Wave on December 12th, 2002. *11th Conference on Mesoscale Processes,* Albuquerque, NM, Amer. Meteor. Soc., TBD.

Yamada, Tetsuji and George Mellor. 1975: A Simulation of the Wangara Atmospheric Boundary Layer Data. *J. Atmos. Sci*., **32**, 2309–2329.

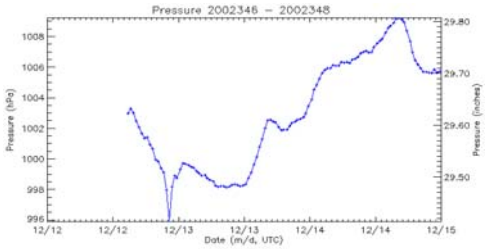

Figure 1. GPS mean sea level pressure (mb) from Palestine, Texas valid from 12/0100 UTC – 15/0000 UTC December 2002.

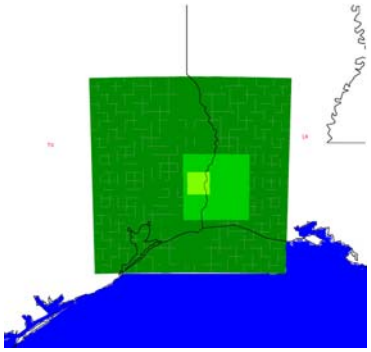

Figure 2. Domain locations for 6kn, 2 km, 667m, 222m, and 71m 12 December 2002 Strato-NHMASS Simulations.

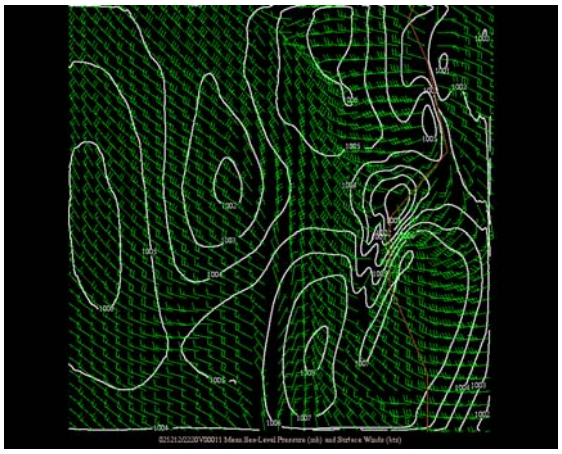

Figure 3. 222m Strato NH-MASS Sea level pressure (white contours) and surface winds (green barbs) valid ~2230 UTC 12 December 2002.

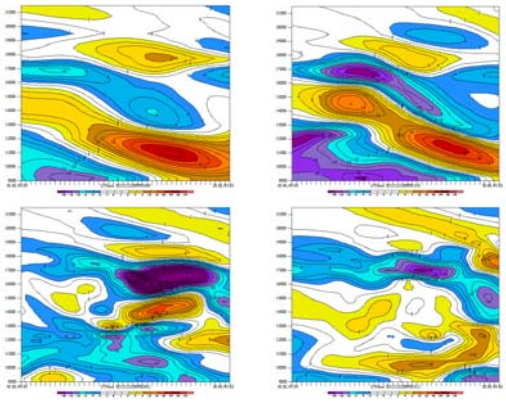

Figure 4. Strato-NHMASS 222m 12 December 2002 U-prime perturbation field at approximately (a) 2219 UTC (b) 2224 UTC (c) 2229 UTC (d) 2234 UTC. Perturbation flow is color filled and contoured in knots.

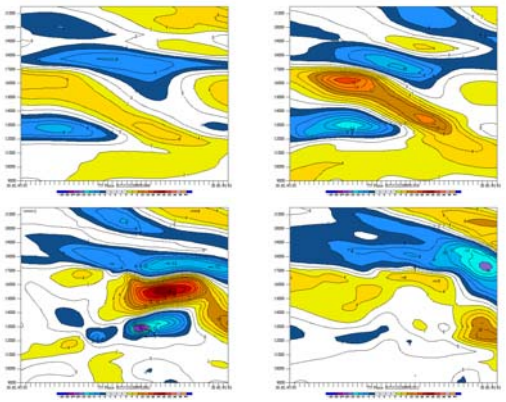

Figure 5. Strato-NHMASS 222m 12 December 2002 virtual potential temperature perturbation field at approximately (a) 2219 UTC (b) 2224 UTC (c) 2229 UTC (d) 2234 UTC. Perturbation flow is color filled and contoured in Kelvin.

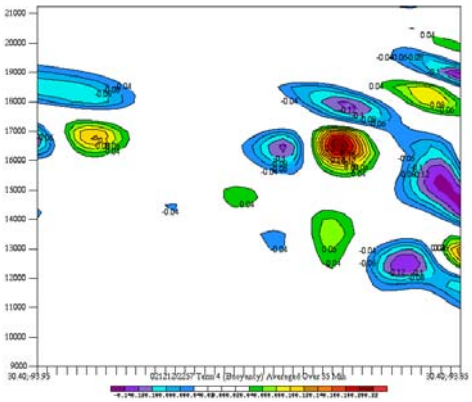

Figure 6. Strato-NHMASS 222m 12 December 2002 1-segment TKE budget showing contribution from Term 4: Buoyant Production (m^2/s^3), averaged over the 35-min model run initialized at 2209 UTC 12 December 2002. The left axis is height in meters. The area of concern is between 16-18 km in the east-central portion of the cross section, where the stratospheric wave breaks. Warm colors correspond to positive contributions, and cool colors correspond to negative contributions.

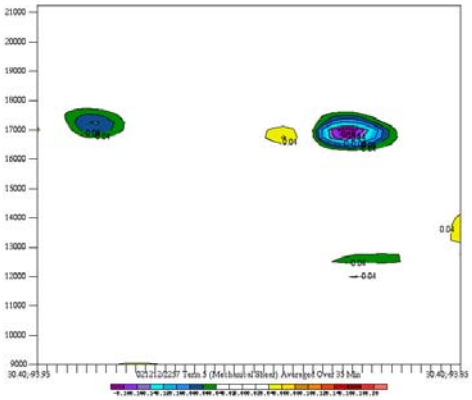

Figure 7. As with Fig. 6, but for Term 5: Mechanical Shear (m^2/s^3).

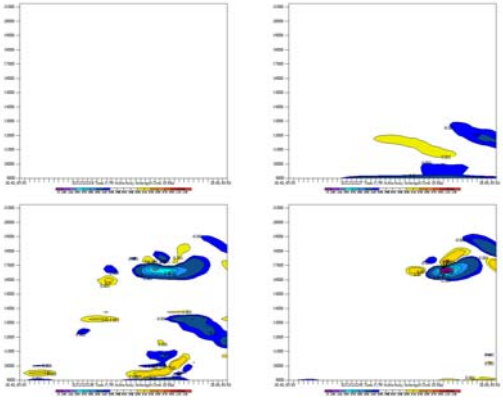

Figure 8. Strato-NHMASS 222m 12 December 2002 4-segment TKE budget showing the evolution of Term 3: W-Advection (m^2/s^3) at approximately (a) 2219 UTC (b) 2224 UTC (c) 2229 UTC (d) 2234 UTC.

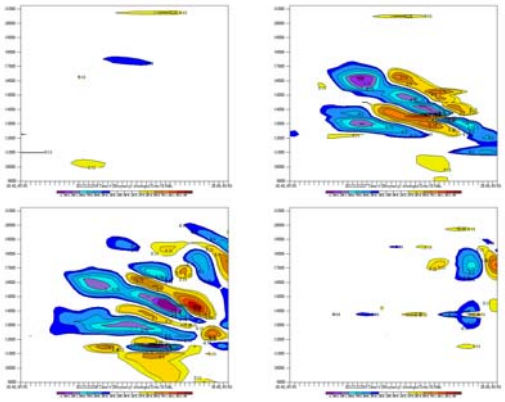

Figure 9. Strato-NHMASS 222m 12 December 2002 4-segment TKE budget showing the evolution of Term 4: Buoyant Production (m^2/s^3) at approximately (a) 2219 UTC (b) 2224 UTC (c) 2229 UTC (d) 2234 UTC.

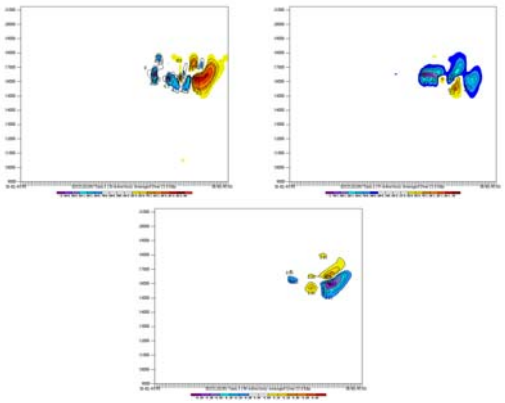

Figure 10. Strato-NHMASS 71m 12 December 2002 1-segment TKE budget showing the evolution of (a) Term 1: U-Advection; (b) Term 2: V-Advection; (c) Term 3: W-Advection. All units are m^2/s^3 and averaged over the 10.5 minute simulation initialized at 2230 UTC 12 December 2002.

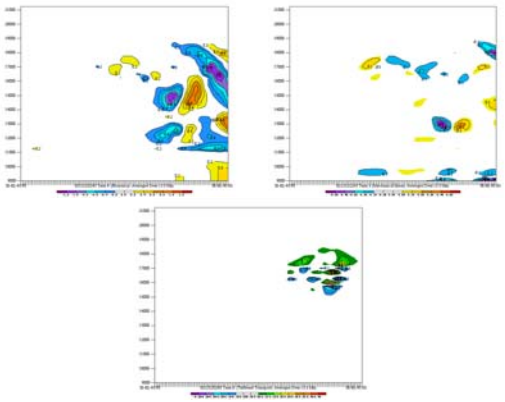

Figure 11. As with Fig. 10, but for (a) Term 4: Buoyant Production; (b) Term 5: Mechanical Shear; (c) Term 6: Turbulent Transport.